Complexities of splashing

COVER ILLUSTRATION

Complexities of splashing

R D Deegan[1], P Brunet[2] and J Eggers[2]

[1] Department of Physics and Center for the Study of Complex Systems, Randall Laboratory, University of Michigan, Ann Arbor, MI 48109, USA
[2] School of Mathematics, University of Bristol, University Walk, Bristol BS8 1TW, UK

Abstract
We study the impact of a drop of liquid onto a thin layer of the same liquid. We give an overview of the sequence of events that occur as the two most important dimensionless control parameters are varied. In particular, multiple cohorts of droplets can be ejected at different stages after impact due to different mechanisms. Edgerton's famous *Milkdrop Coronet* is only observed for a narrow range of parameters. Outside this range, the splash is either qualitatively different, or suffers from a much lower level of regularity.

PACS numbers: 47.20.−k, 47.20.Ma, 47.55.D−

(Some figures in this article are in colour only in the electronic version)

1. Introduction

The ubiquity of splashes, caused by the collision of a fluid drop with a surface, has been argued eloquently by Worthington [1]. Indeed, splashes are one of the main fascinations of fluid mechanics [2]. The detailed sequence of events following impact depends very much not only on the speed and the type of fluid, but also on the substrate. If the substrate is dry, results depend on the smoothness of the surface [3], the wetting angle between solid and liquid [4] and the presence of air [5]. Impact may be into a deep pool of the same liquid [1], or onto a thin layer of the same [6–8] or another liquid [9]. Non-Newtonian liquid behaviour can also change the result qualitatively [10,11].

Edgerton [6] discovered that the impact onto a thin layer results in the most regular structure, the famous *Milkdrop Coronet*. Similar crowns, albeit more disordered, had been found earlier by Worthington when studying impact on a deep pool [12]. As illustrated in figure 1, Edgerton lets a sequence of milk drops fall onto a solid surface to establish a thin layer of liquid. In this paper, by contrast, we carefully control the thickness of the target fluid layer. However, as pointed out by Kadanoff [13], and as illustrated by the cover of this issue and in figure 2, not all events have the same degree of regularity. There are also indications that the regularity seen in Edgerton's photograph arises from the non-Newtonian properties of milk which help to damp perturbations [14].
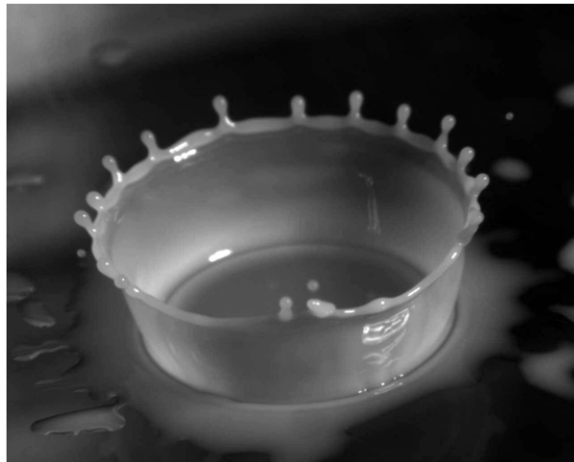
Figure 1. A sequence of milk drops falling on a solid surface.

Figure 2. Impact of propanol drop on the same fluid.

In this paper we illustrate that the regular crown structure found by Edgerton is a rare exception, observed only in a narrow range of parameters. As we show in more detail below, the formation of an Edgerton milk crown results from an intricate sequence of events. First, a cylindrical fluid sheet shoots out from the layer, forming a fat rim. Second, cylindrical symmetry is broken by a linear instability of the rim, which selects a preferred wavelength at which the thickness of the rim varies periodically. Third, in a nonlinear stage of the original instability, the rim develops tips, from which jets emanate. Fourth, drops pinch off from the end of each jet. Irrespective of its regularity, we herein call the generation of droplets by this mechanism a **crown splash**.

In practice, a whole range of other phenomena can take place as one moves outside the light shaded region of figure 3. In particular, there are at least two separate mechanisms by which sheets form upon impact, and the end products of the impact event are strongly influenced by whether these sheets decay separately, commingle or interact. The symmetry breaking instability of each sheet may occur by one or more mechanisms, leading to noisy structures in general.
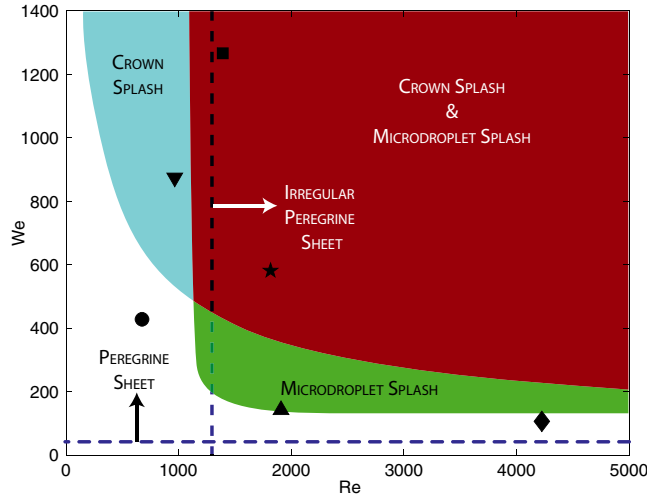
Figure 3. Phase diagram indicating the qualitatively different regimes of drop impact. The dashed vertical line indicates the Re beyond which the Peregrine sheet is disordered, and the horizontal dashed line indicates the We number above which a Peregrine sheet forms.

Our study is meant to elucidate the complexities of drop impact onto a thin layer, by pointing out the existence of different structures in different ranges of the space of control parameters. Failing that, it is impossible to appreciate the distinct dynamical origins of secondary droplets.

To a very good approximation, our experiments represent a spherical drop of a Newtonian liquid, of diameter D, impacting with velocity U onto a fluid layer of thickness h of the same liquid. For all our experiments, h is fixed at $0.2D$. More details of possible deviations from a spherical shape, influence of air, etc are discussed in the experimental section.

Conventional dimensionless parameters are the Weber number, Reynolds number, Froude number and the dimensionless thickness of the layer:

$$\mathsf{We} = \frac{\rho D U^2}{\gamma}, \qquad \mathsf{Re} = \frac{DU}{\nu}, \qquad \mathsf{Fr} = \frac{U^2}{gD}, \qquad \mathsf{H} = \frac{h}{D}. \qquad (1)$$

The most important parameters are the Weber number (We) and the Reynolds number (Re). Gravity is negligible as indicated by the typical Froude number of 10^2, and we will therefore disregard it. The layer thickness h plays a small role on a quantitative level, but does not affect things qualitatively, as long as one stays within the realm of thin layers.

2. Experiments

In our experiments a drop was produced from a bevelled hypodermic needle (gauge 21, 26 or 30) held at a fixed height 20–120 cm above a liquid bath, as shown in figure 4. The needle was gravity fed from an open reservoir. The waiting time between two drop impacts was set to be more than 10 s, to allow the layer to recover a flat horizontal shape. The target layer was formed in the bath between the liquid surface and a 4 in. diameter, $\lambda/4$, glass, optical flat (Edmund optics). The bottom of the bath was also glass, permitting an unimpeded view of the impact from below. The layer depth was measured using a needle mounted on a micrometer to locate the liquid surface and the solid substrate. Depending on the drop size this ranged from 290 to 580 μm and was uniform to within $\pm 10\,\mu$m.
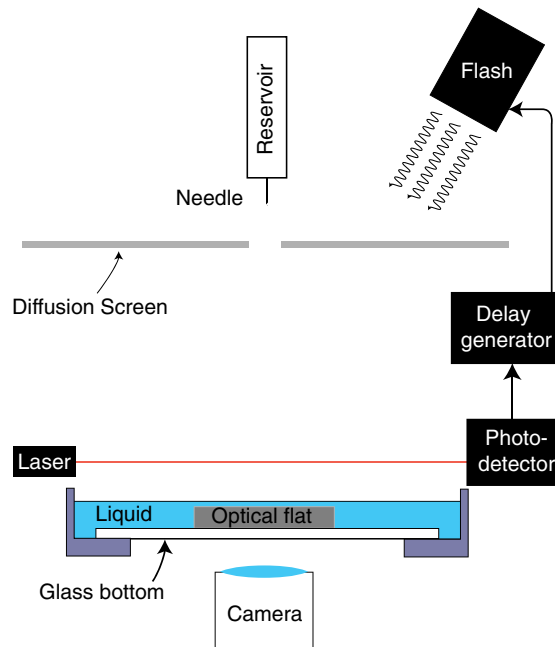
Figure 4. Experimental apparatus.

Images were acquired with either a high speed video camera (Phantom 5.0, Vision Research Inc.) or with a still camera (Canon 20D SLR). Back-lighting was used throughout and provided by two 500 W halogen lamps for filming or by a 6 J, 500 ns flash (Palflash 501, Pulse Photonics Ltd). The flash was triggered by the drop cutting a collimated laser sheet focused onto a photo-detector. A home-made delay generator enables us to take pictures at a desired time after impact. The reproducibility of the image capture was $\pm 10\,\mu$s. Due to the back-lighting the drop obscured the earliest times after impact. The high speed video camera was typically set to capture a $10\,\mu$s exposure, with a resolution of 512×256 pixels at 7400 frames per second. The advantage of taking single flash photographs was the much improved spatial and temporal resolution.

We used propanol, water, silicon oil and a 32/68 w/w mixture of glycerol and water. The values for the fluid properties used to calculate Re and We are given in table 1. The diameter of the drops was calculated from the weight of the drops, and the speed of the drop before impact was measured from video footage. Drops with diameters 1.4–2.9 mm were generated using different gauge needles. For all drop sizes the oscillations caused by the drop pinch died off quickly. For larger drops, though, the leading surface of the drop was flattened by air drag. Except just prior to impact, drops smaller than 2.0 mm were spherical to within our capacity to measure. At impact all drops develop a small concavity on the leading surface due to the strong lubrication pressure as air is squeezed out from between the drop and the impact layer [15]. The speed at impact was increased by raising the fall height, and was noticeably slowed by air drag.

3. Two types of sheets

There are at least two types of sheets, of completely different physical origin, produced when the drop hits the fluid layer. We will discuss them in turn.

Table 1. Properties of fluids used in our experiments.

| Fluid	ρ (g cm^{-3})	η (cP)	γ (dyn cm^{-1})
Water	1.00	1.0	75
Propanol	0.79	2.4	23
Silicon oil	0.92	5.2	21
Glycerol/water mixture	1.08	2.9	73
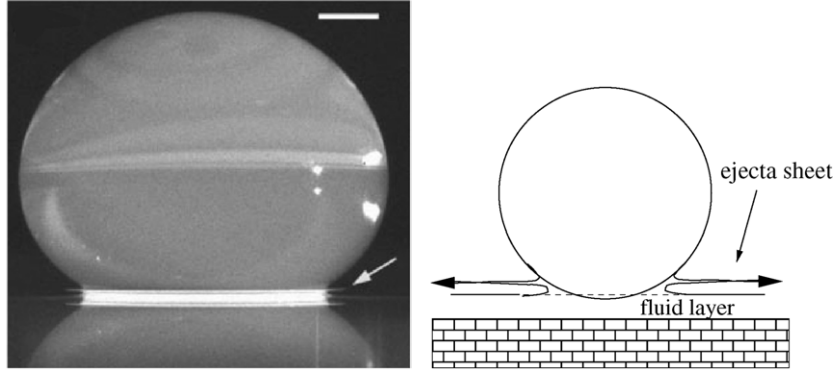
Figure 5. *Left*: an experimental snapshot of a drop directly after impact [15] (reproduced courtesy of Cambridge University Press). The parameters are Re = 1080, We = 4170. *Right*: a diagram of the same process, following [17]. An ejecta sheet shoots out horizontally from underneath the drop.

3.1. Ejecta sheet

This sheet, first observed experimentally by Thoroddsen [15] and seen in numerical simulations by [16] is produced at the moment of impact. An example is shown in figure 5. As the drop touches the surface at finite speed, a localized pressure singularity is produced, pushing fluid outwards. From the symmetry of the problem at the first moment of impact it is clear that the sheet must shoot out horizontally, and that equal amounts of drop and layer fluid are contained in it.

A theory of the ejecta sheet was presented in [17], neglecting both surface tension and viscosity. Thus both the Reynolds and Weber numbers are infinite. In this limit, there is no time scale to the problem, and the sheet instantaneously reaches infinity. As the drop penetrates the layer, the sheet thickens and a larger percentage comes from the layer fluid. Clearly, in reality the ejecta sheet cannot shoot out to infinity, and certainly not in zero time; restoring surface tension to the problem, as was done in simulations of [16], yields a finite speed (see figures 4–6 in [16]). Ejecta sheet speeds were measured experimentally by [15], and show increasingly high speeds with decreasing viscosity, reaching up to 50 m s^{-1}.

Weiss and Yarin [16] also investigate the role of surface tension for the *existence* of an ejecta sheet. They find that for We < 40 no ejecta sheet is produced at all. Rather, the motion is transformed into a capillary wave that runs along the drop. In our experiments, we observe small droplets long before the crown splash but we do not have the resolution to observe the mechanism by which these are generated. In our phase diagram, all such cases are lumped together with the label **microdroplet splash**. Nonetheless, if we assume that these microdroplets originate in the breakup of the ejecta sheet then our boundary at high Re approaches We = 130 in fair agreement with Weiss and Yarin's result of We $\approx$ 40 for Re $\rightarrow \infty$.
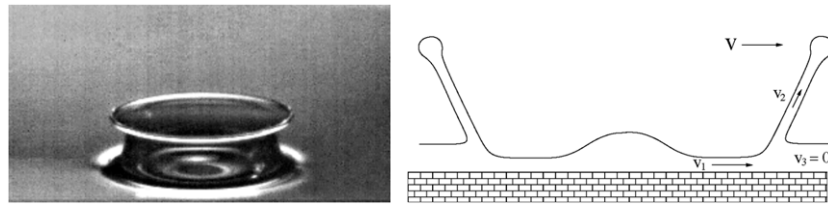
Figure 6. *Left*: an experiment corresponding to the diagram on the right. The parameters are $\mathsf{Re} = 676$, $\mathsf{We} = 428$, $775\,\mu$s after impact. Corresponds to ● in figure 3. *Right*: a diagram of the mechanism for sheet formation as proposed in [2]. Mass and momentum conservation determine the velocity and angle of the upward moving sheet, which usually rises at a steep angle.

Figure 7. An ejecta sheet 'riding' on a Peregrine sheet. The former leads to the formation of tiny droplets that precede the much larger Peregrine sheet. $\mathsf{Re} = 1354$, $\mathsf{We} = 874$, $580\,\mu$s after impact. Corresponds to ★ in figure 3.

3.2. Peregrine sheet

After the drop has penetrated the layer, a sheet of liquid travels outwards over the solid surface. It collides head on with the as-yet unmixed fluid in the preexisting layer. This mechanism, first described by Peregrine [2], is illustrated in figure 6. Elementary considerations of mass and momentum balance show that, given the thicknesses and velocities of the two incoming sheets (in the frame of reference of the moving base), that the speed, thickness and ejection angle of the resulting sheet can be calculated. An experimental example is shown in figure 6. Peregrine sheets form for $\mathsf{We} > 40$, and are disordered from the earliest observable times for $\mathsf{Re} > 1300$. These features are, respectively, denoted by dashed horizontal and vertical lines in figure 3.

3.3. Combination of two sheets

This qualitative breakdown of the splash is summarized in figure 3. For most of the parameter regime of our experiments, the two sheets described appear together in any given impact event. We are aware of three different fates of the ejecta sheet.

  (i) The ejecta sheet becomes the leading edge of the Peregrine sheet, as the latter grows underneath the former. In figure 7 we show a Peregrine sheet, whose rim has not yet broken up. Yet a number of very small drops precede the rim. These form from a horizontal sheet attached to the rim at early times.
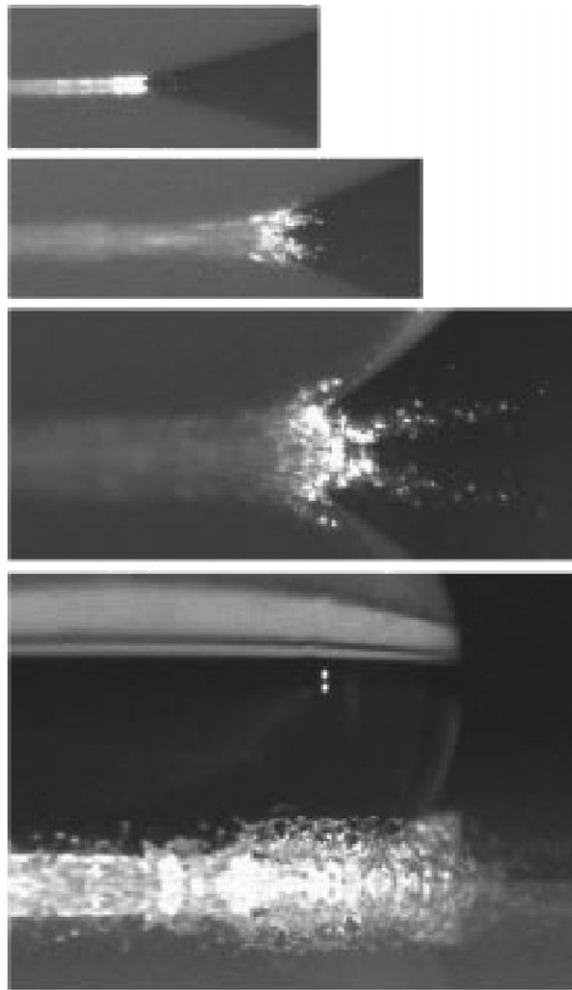
Figure 8. An ejecta sheet breaking up into many smaller droplets, at a stage where the sheet is still hidden completely underneath the drop [15] (reproduced courtesy of Cambridge University Press). The parameters are $Re = 2.9 \times 10^4$ and $We = 1.8 \times 10^3$.

(ii) The ejecta sheet collides with the fluid layer, trapping pockets of air in substrate liquid. We have observed a circular residue of bubbles surrounding the impact centre that persist long after impact. Weiss and Yarin [16] observe this process in their numerical calculations.

(iii) The ejecta sheet breaks up immediately (the so-called **prompt splash**; see figure 8). This may lead to additional irregularity of the Peregrine sheet and kick start the rim instability.

4. Symmetry breaking

The initial configuration is cylindrically symmetric, yet most final configurations break this symmetry. This indicates the existence of one or more instabilities, which break the symmetry. This is surely the case for the prompt splash shown in figure 8, which suggests almost instantaneous breakup into many very small droplets. There may be many more instabilities
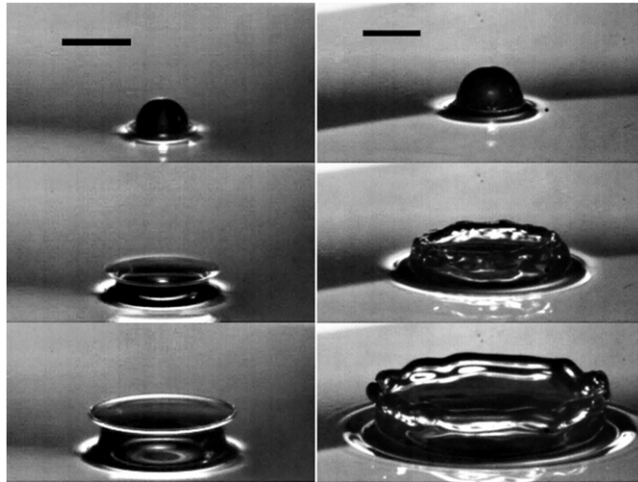
Figure 9. Smooth and disordered Peregrine sheets that do not produce secondary droplets. *Left*: silicon oil, Re = 676, We = 428, H = 0.2 at 100, 368, 775 μs after impact. Corresponds to circle in figure 3. *Right*: water, Re = 4226, We = 106, H = 0.2 at 300, 1650, 4215 μs after impact. Corresponds to ◆ in figure 3. Scale bar corresponds to 2 mm.

associated with the ejecta sheet, but we will not elaborate here, since we have few original data to report.

We begin by remarking that the symmetry is not *necessarily* broken, at least not to a degree that is measurable experimentally. An example of this situation is shown in the series of panels in figure 9 (*left*). A Peregrine sheet develops a rim, but even as the rim falls back into the layer, no instability is observed.

A different variant of the same situation is seen on the right of the same figure, for an impact that takes place at much higher Re (see the phase diagram in figure 3). Although the rim never breaks up, the flow is irregular from the earliest times of observation. A possible explanation is that the high Reynolds number introduces turbulence into the flow.

The sequence in figure 10 (*left*) corresponds to Edgerton's crown (figure 1) described above. First, a Peregrine sheet is formed, which only turns unstable at its rim, owing to a varicose instability. The wavelength selection associated with this Rayleigh–Plateau instability will be investigated in more detail in a future publication. Note in particular that fluctuations in the local wavelength remain as one goes around the rim.

As the perturbations grow in size, modest local variations of the rim radius turn into spikes, pointing away from the sheet. We have confirmed that apart from a slight coarsening (merging of two spikes), the initial linear instability sets the number of tips (jets) on the crown. Most jets shed a drop from their end, so the initial instability is also crucial for the determination of the number of drops.

In figure 10 (*right*) drops are produced as well, but of a far smaller size. The rim of the Peregrine sheet develops an instability, but does not grow enough to lead to drops. However, drops have been produced close to the moment of impact. We suspect the process of drop formation is analogous to what is shown in figure 8. Thus the drops seen in the later stages of the sheet formation in figure 10 (*right*) are simply a remnant of an essentially unrelated event.

The image on the cover highlights the role of noise in the generation of droplets. The experimental conditions (Re = 861, We = 673, H = 0.079) were such that secondary droplets

Figure 10. *Left*: crown splash without a microdroplet splash. Silicon oil, $\mathsf{Re} = 966$, $\mathsf{We} = 874$, $\mathsf{H} = 0.2$ at 200, 740, 1410, 2430 μs after impact. Corresponds to ▼ in figure 3. *Right*: microdroplet splash without a crown splash. Glycerol/water mixture, $\mathsf{Re} = 1910$, $\mathsf{We} = 142$, $\mathsf{H} = 0.2$ at 260, 940, 1780, 6880, 11200 μs after impact. Corresponds to ▲ in figure 3. Scale bar corresponds to 2 mm.

would not ordinarily form. This particular impact event produced droplets because of an initial inhomogeneity in the experimental conditions. Though we could not identify the source of the inhomogeneity, we can reproduce the structure by placing a small obstacle at the impact site. The head start provided by the initial perturbations allows the rim of the Peregrine sheet to reach the nonlinear stage of droplet ejection sooner than it would have otherwise. The sensitivity of drop generation to the initial conditions illustrates the difficulty of disentangling the instability of the ejecta sheet from the instability of the Peregrine sheet when the former interacts with the early stages of the latter.

Two more types of splashes are shown in figure 11. To the left we show a combination of small and large drops. The large drops come from the rim instability of the Peregrine sheet as described before, although the process is perhaps slightly more irregular. However, superimposed on this structure a number of much smaller drops are visible. These form from a horizontal sheet attached to the Peregrine sheet at early times.

The right-hand side of figure 11 shows yet another phenomenon. The end of the Peregrine sheet may be significantly curved (also seen by [15]). We are not sure what causes this curvature but some possibilities are

 (i) A time dependence of the ejection angle of the sheet [2]. The bending of the sheet may therefore be a purely kinematic effect.
 (ii) The intrinsic dynamics of the sheet due to the action of surface tension, akin to the behaviour of an *elastic* sheet.
(iii) The effect of air.
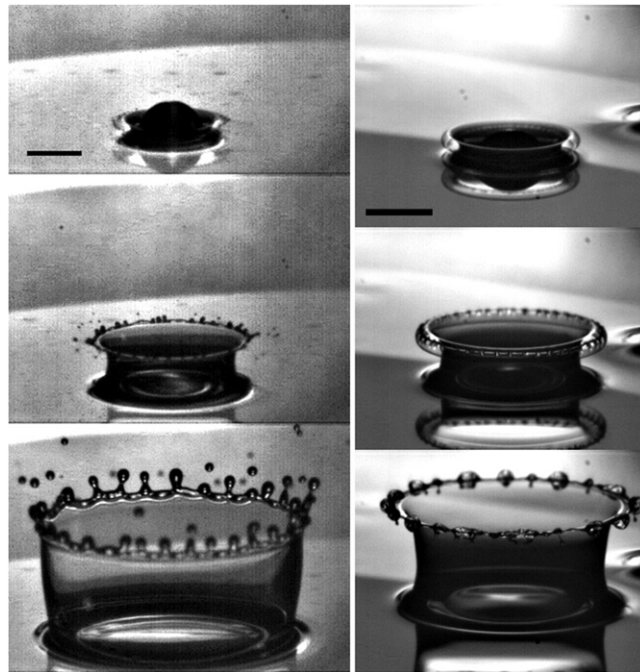
Figure 11. *Left*: drop impact producing both a microdroplet and crown splash. Propanol, Re = 1816, We = 582, H = 0.2 at 160, 570, 2650 μs after impact. Corresponds to ★ in figure 3. *Right*: splash which entrains bubbles in to the Peregrine sheet rim. Silicon oil, Re = 1392, We = 1326, H = 0.2 at 200, 610, 1010 μs after impact. Corresponds to ■ in figure 3. The scale bar corresponds to 2 mm.

In figure 11 (*right*) the bending becomes so pronounced that the sheet closes in on itself, and bubbles are entrained, as seen in the last photograph of the sequence.

In summary, we have shown that there are at least three sources of secondary droplets:

(i) A prompt instability of the ejecta sheet which occurs immediately upon impact and produces very small droplets. Figure 8 shows an example of this splash.

(ii) A rim instability of the ejecta sheet which produces medium-sized droplets. An example is given in figure11.

(iii) A rim instability of the Peregrine sheet which produces large droplets. This is referred to as crown splash in figure 3. The boundary of this regime follows the simple relationship We · Re$^{0.5}$ = c with $c = 2.6 \times 10^4$, which agrees well with experimental observation as shown in figure 12. Curiously, the same correlation has been proposed in [18] for dry surfaces (but with a much smaller value of c), for which there is no Peregrine sheet. Similar correlations have also been found in [19] for impact on thin films, but without specifying the mechanism by which drops are produced.

These mechanisms are typically interdependent and with the earlier ones influencing the later ones. The phase diagram shown in figure 3, though still incomplete, reflects some of the complexities that arise from the interaction of these mechanisms.
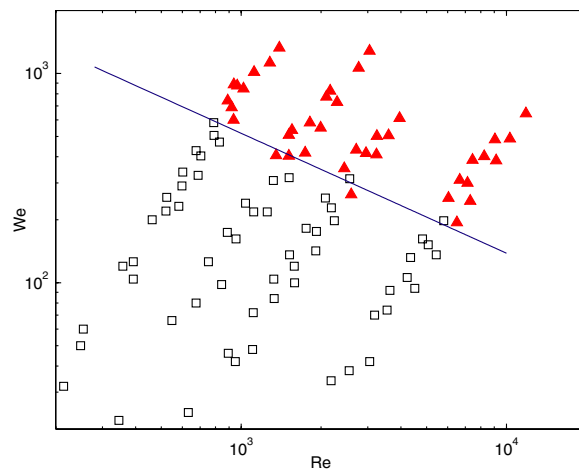
Figure 12. Drop impacts with (▲) and without (□) a crown splash. The solid line is a fit to the boundary using the power law $\mathsf{We} = c\,\mathsf{Re}^{-0.5}$, yielding $c = 2.6 \times 10^4$.

Acknowledgment

References

[1] Worthington A M 1908 *A Study of Splashes* (London: Longmans)
[2] Peregrine D H 1981 *J. Fluid Mech.* **106** 59
[3] Xu L, Barcos L and Nagel S R 2006 *Preprint* physics/0608079
[4] Sikalo S, Wilhelm H D, Roisman I V, Jakirlic S and Tropea C 2005 *Phys. Fluids* **17** 062103
[5] Xu L, Zhang W W and Nagel S R 2005 *Phys. Rev. Lett.* **94** 184505
[6] Edgerton H E 1977 *Stopping Time: The Photographs of Harold Edgerton* (New York: Abrams)
[7] Josserand C and Zaleski S 2003 *Phys. Fluids* **15** 1650
[8] Yarin A L 2006 *Ann. Rev. Fluid Mech.* **38** 159–92
[9] Thoroddsen S T, Etoh T G and Takehara K 2006 *J. Fluid Mech.* **557** 63–72
[10] Bergeron V, Bonn D, Martin J Y and Vovelle L 2000 *Nature* **405** 772–5
[11] Rozhkov A, Prunet-Foch B and Vignes-Adler M 2006 *J. Non-Newtonian Fluid Mech.* **134** 44
[12] Kemp M 1998 *Nature* **396** 633
[13] Kadanoff L P 2000 *Univ. Chicago Rec.* **35** 2
[14] Vignes-Adler M 2004 *Talk delivered at Euromech 450 (Marseille)*
[15] Thoroddsen S T 2002 *J. Fluid Mech.* **451** 373
[16] Weiss D A and Yarin A L 1999 *J. Fluid Mech.* **385** 229
[17] Howison S D, Ockendon J R, Oliver J M, Purvis R and Smith F T 2005 *J. Fluid Mech.* **542** 1
[18] Mundo C, Sommerfeld M and Tropea C 1995 *Int. J. Multiph. Flow* **21** 151
[19] Vander Wal R L, Berger G M and Mozes S D 2006 *Exp. Fluids* **40** 33